Applied Catalysis B: Environmental 182 (2016) 1–14

Contents lists available at ScienceDirect

Applied Catalysis B: Environmental

journal homepage: www.elsevier.com/locate/apcatb

# Effect of Cu additives on the performance of a cobalt substituted ceria ($Ce_{0.90}Co_{0.10}O_{2-\delta}$) catalyst in total and preferential CO oxidation

Thandanani Cwele, N. Mahadevaiah, Sooboo Singh, Holger B. Friedrich*

*Catalysis Research Group, School of Chemistry and Physics, University of KwaZulu-Natal, Westville Campus, Durban 4000, South Africa*

ARTICLE INFO

*Article history:*
Received 9 April 2015
Received in revised form 26 August 2015
Accepted 27 August 2015
Available online 29 August 2015

*Keywords:*
CO–PROX
CO oxidation
Ceria
Solid-solution
Cu–Co-containing catalysts

ABSTRACT

The study reports the modification of the developed $Ce_{0.90}Co_{0.10}O_{2-\delta}$ catalyst by incorporating copper ions in order to improve the catalytic activity for total and preferential CO oxidation (TOX and PROX). A series of metal ion substituted ceria catalysts, $Ce_{0.90}Co_{0.10}O_{2-\delta}$ and $Ce_{0.90-x}Cu_xCo_{0.10}O_{2-\delta}$ ($x = 0.01$, 0.03 and 0.05) were synthesized in a single step by the urea-assisted solution combustion method. The compositions, textural and structural properties of the catalysts were characterized by XRD, XPS, Raman, $H_2$-TPR and ICP-OES. The insertion of Cu ions in $Ce_{0.90}Co_{0.10}O_{2-\delta}$ greatly enhanced the reducibility and improved the activity, with especially the $Ce_{0.85}Cu_{0.05}Co_{0.10}O_{2-\delta}$ catalyst showing superior catalytic performance compared to other bimetallic catalysts. Analysis of the reaction profiles and rate calculations suggest that $H_2$ and CO oxidation over $Ce_{0.90}Co_{0.10}O_{2-\delta}$ may be occurring on the same active sites, while the two reactions appear to be taking place on independent sites over the Cu-containing catalysts. In addition, the effect of $H_2O/CO_2$ in PROX has been studied. The degree of deactivation by $H_2O$ and $CO_2$ decreased with increasing the Cu content in the catalysts. The presented catalysts are highly active, selective and stable in TOX and PROX.



## 1. Introduction

In the context of growing environmental concerns and interest in the development of clean energy alternative technologies, polymer electrolyte membrane fuel cells (PEMFCs) have become an important subject of research aimed at addressing energy-related concerns. This is due to their low temperature of operation, reasonably high power density and zero emission of pollutants [1]. Most of the hydrogen required as fuel for PEMFCs is produced by steam reforming of hydrocarbon fuels, followed by the water gas shift (WGS) reaction, in order to improve hydrogen yield. The hydrogen produced after this step co-exists with ca.1% of carbon monoxide (CO) and other gaseous products [2]. This amount of CO in the hydrogen stream drastically decreases the efficiency of the Pt anode catalyst in converting hydrogen fuel to energy [3,4]. Therefore, the removal of CO from the reformate gas is necessary in order to ensure maximum PEMFC power output. To date, CO preferential oxidation is one of the most effective ways for the purification of the reformate stream, with minimal hydrogen consumption [5].

Different types of catalyst formulations have been explored and studied for the total CO oxidation (TOX) and preferential CO oxidation (PROX) [6,7]. Among other transition metals, platinum group metal (PGM) based catalysts have been widely studied and applied for PROX. As early as the 1960s, $Pt/Al_2O_3$ catalysts were used by the Engelhard Corperation in hydrogen plants to remove CO prior to ammonia synthesis [8]. Since then, more catalysts have been developed to purify hydrogen for PEMFC applications. The most studied PGMs are Pt and Pd and to a lesser extent Rh and Ru, supported on materials such as silica, alumina, zeolites and ceria [9].

Ceria-based materials are well known for their applications as oxygen storage materials in automotive three-way catalytic converters (TWC), also these catalysts have gained recognition in a wide range of applications, most notably in solid oxide fuel cells, low-temperature WGS and CO oxidation reactions [10,11]. The catalytic behaviour demonstrated by ceria-based materials is often attributed to their good ionic conduction, temperature stability and the facile redox cycle between $Ce^{3+}$ and $Ce^{4+}$ [12]. Total CO oxidation and preferential CO oxidation have received more attention over these materials due to their applications in emission control and fuel cell technologies [13–15]. In most cases, ceria has been used as a support for active precious metals, such as Pt, Au or Pd [15–17]. Despite good CO oxidation activity shown by these catalysts, the drawback is that they are also active for the undesirable $H_2$ oxidation reaction.

* Corresponding author. Fax: +27 31 2603091.
*E-mail address:* friedric@ukzn.ac.za (H.B. Friedrich).

http://dx.doi.org/10.1016/j.apcatb.2015.08.043
0926-3373/

Many researchers have investigated the catalytic performance of non-precious transition metal oxide catalysts for TOX and PROX [18–20]. Among the explored metal oxides, copper and cobalt based oxides, especially CuO and $Co_3O_4$, are the most promising catalysts for TOX and PROX [21]. Ceria-supported copper catalysts have been widely used as alternative catalyst formulations for these reactions. The good activity of CuO–$CeO_2$ catalysts has been attributed to the synergistic interaction between Cu and Ce, as represented by a proposed redox equilibrium, $Ce^{4+} - Cu^{1+} \leftrightarrow Ce^{3+} - Cu^{2+}$ [18,19,22–24]. The importance of the alternating between Cu(I) and Cu(II) oxidation states has been emphasized by Jernigan and Somorjai [25]. On the other hand, in the case of unsupported $Co_3O_4$, its activity has been associated with the co-existence of $Co^{2+} - Co^{3+}$ pairs [26]. Unfortunately, pure $Co_3O_4$ deactivates easily, especially in the presence of moisture and is only efficient for low-temperature total CO oxidation [27]. In a $H_2$-rich stream, the Co species, in bulk $Co_3O_4$, can be reduced to $Co^{2+}$ and $Co^0$ which are not active for CO oxidation [28,29].

Motivated by the performance of the CuO–$CeO_2$ system, several researchers have studied the activity of $Co_3O_4$–$CeO_2$ catalysts [30–33]. It has been shown that, when supported on oxides, $Co_3O_4$ catalysts can maintain their good PROX activity due to the enhancement of the $Co^{2+} - Co^{3+}$ redox potential [33]. PROX studies of $Co_3O_4$–$CeO_2$ catalysts have shown that the activation energy of CO oxidation is always lower than that of $H_2$ oxidation [31]. Regardless of better stability, compared to pure $Co_3O_4$, supported $Co_3O_4$ catalysts suffer from deactivation in excess $H_2$ due to the formation of CoO and have low tolerance for $CO_2$ and $H_2O$ [34,35].

Although the catalytic behaviour of supported metal oxide catalysts is positively influenced by a strong interaction between the support and the active phase, one of their pitfalls is that the entirety of the supported component is not involved in catalytic conversion. This drawback is often associated with incomplete dispersion of the active phase, which is important for strong interaction and enhanced activity [33,36]. A recent approach to improve interaction involves doping active metals into the matrix of the support, ceria [37,12]. The resulting material is a uniform solid-solution catalyst with modified redox properties and which contains defects, which are significant for oxidation reactions. In some cases, such catalysts have shown improved activity compared to metal supported catalysts [38,39]. With the intention of ensuring maximum interaction of Co with Ce, a nanocrystalline $Ce_{0.90}Co_{0.10}O_{2-\delta}$ catalyst has been synthesised, where the cobalt ions are incorporated into the ceria lattice. To improve the robustness of the catalyst in the presence of $CO_2$ and $H_2O$, the promotional effect of Cu was investigated by employing new $Ce_{0.90-x}Cu_xCo_{0.10}O_{2-\delta}$ (where $x = 0.01$, 0.03 and 0.05) catalysts. In the present work, structural studies of the prepared catalysts and their catalytic performance in CO oxidation and PROX are reported for the first time.

## 2. Materials and methods

### 2.1. Preparation of the catalysts

The nanocrystalline solid solution catalyst, $Ce_{0.90}Co_{0.10}O_{2-\delta}$, was prepared using a single-step combustion method [12]. All the metal precursors and chemicals used in the preparation of the catalysts were procured from Sigma-Aldrich with purity 99.9%. In the preparation, a redox combustion mixture was composed of $(NH_4)_2Ce(NO_3)_6$, $Co(NO_3)_2.5H_2O$ and $NH_2CONH_2$ in the ratio of 0.90: 0.1: 3.77 respectively. Typically, a mixture of 9.869 g of $(NH_4)_2Ce(NO_3)_6$, 0.582 g of $Co(NO_3)_2.5H_2O$ and 4.529 g of $NH_2CONH_2$ was dissolved in 50 $cm^3$ of water in a borosilicate dish. The resulting solution was heated at 150 °C on a hotplate for 10 min. The boiling solution was then transferred into a muffle furnace, preheated to 400 °C. After almost complete dehydration, the slurry ignited, resulting in the formation of a brown solid product. A similar one-step combustion method was used to prepare the $Ce_{0.90-x}Cu_xCo_{0.10}O_{2-\delta}$ (where $x = 0.01$, 0.03 and 0.05) bimetallic solid solutions, using $Cu(NO_3)_2.3H_2O$ as a precursor, in addition to the other starting materials mentioned in the preparation of $Ce_{0.90}Co_{0.10}O_{2-\delta}$. Pure ceria nanopowder was also prepared by the solution combustion method, using a cerium ammonium nitrate-urea redox mixture. The $Co_3O_4$ used for the preparation of a physical mixture, 10%$Co_3O_4$/$CeO_2$, was prepared by precipitation and calcined at 400 °C for 4 h [40]. The physical mixture was prepared by dry-grinding the two pure oxides, followed by calcining at 400 °C for 4 h.

### 2.2. Catalyst characterization

The textural properties, such as BET surface area, pore volume and pore size of the catalysts were determined from the adsorption and desorption isotherms of nitrogen at −196 °C using a Micromeritics TriStar 3000 multipoint analyzer. X-ray powder diffraction (XRD) experiments were performed on a Bruker D8 Advance diffractometer equipped with an XRK900 in situ cell and a Cu Kα source (λ = 1.5406 Å). The XRD patterns were recorded in the $2\theta$ range of 10–90° at a scan rate of 0.5°/min, with a step width of 0.02°. The XRD patterns were refined by the Rietveld method using the Full Prof Suite-2000 program. Transmission electron microscopy (TEM) was performed on a Jeol JEM-1010 electron microscope and the images obtained were further analyzed using iTEM software. High resolution TEM (HR-TEM) was carried out on a JEM-2100 electron microscope. Samples were prepared by dispersing them in ethanol before they were deposited onto holey carbon-coated grids. The field emission scanning electron microscope (FEG-SEM) images were captured using a ZEISS FEG-SEM Ultra Plus instrument. Raman spectroscopy analysis was conducted using an Advantage 532 series spectrometer, equipped with the visible laser line of 514 nm. X-ray photoelectron measurements were performed with a Thermo Scientific Multilab 2000 apparatus using Al Kα radiation (1486.6 eV) and the C (1s) spectra as the reference (284.5 eV) for all binding energies. For the pre-reduced sample, the sample was pre-treated at 600 °C for 4 h under a flow of hydrogen. The sample was then cooled to room temperature under hydrogen and immediately prepared for analysis in a secluded chamber. Inductively coupled plasma (ICP) was carried out using a Perkin Elmer Optical Emission Spectrometer Optima 5,300 DV and the standards (1,000 ppm Ce, Cu and Co) were obtained from Fluka. Hydrogen temperature-programmed reduction ($H_2$-TPR) experiments were carried out on a Micromeritics AutoChem II 2920 Chemisorption analyzer equipped with a thermal conductivity detector (TCD). In these experiments, the sample (∼30 mg) was pre-treated under a flow of argon at 400 °C for 30 min, followed by cooling to room temperature before any runs were carried out. The OSC (oxygen storage capacity) of all the catalysts were studied by $H_2$-TPR or hydrogen uptake measurements. $H_2$ uptake measurements were performed repeatedly by reducing the compound in $H_2$ up to 550 °C followed by oxidation in $O_2$ at 400 °C over several cycles and no changes in the structure of the material during this redox process was observed.

### 2.3. Catalytic activity measurements

The catalytic behaviour of the catalysts was evaluated in the gas phase at atmospheric pressure and a temperature range from ambient to 250 °C. All gases used were analytical grade and were received from Afrox or Air Products. The gases were purified by a solid trap of molecular sieves to ensure that no water passed to the mass flow controllers (MFC) and subsequently to the reac-

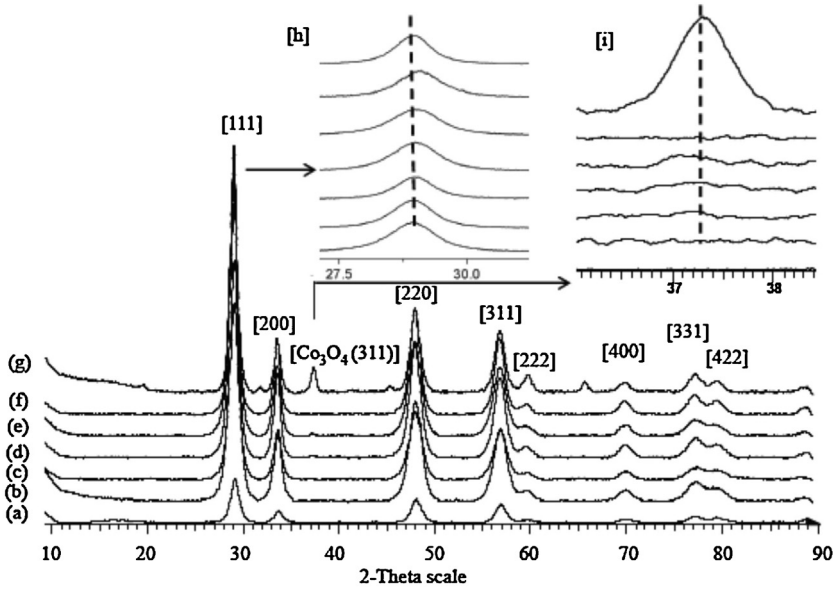


**Fig. 1.** X-ray diffraction patterns of (a) $CeO_2$, (b) $Ce_{0.9}Co_{0.10}O_{2-\delta}$, (c) $Ce_{0.89}Cu_{0.01}Co_{0.10}O_{2-\delta}$, (d) $Ce_{0.87}Cu_{0.03}Co_{0.10}O_{2-\delta}$, (e) $Ce_{0.85}Cu_{0.05}Co_{0.10}O_{2-\delta}$, (f) $Ce_{0.95}Cu_{0.05}O_{2-\delta}$ and (g) 10% $Co_3O_4/CeO_2$ .The insets show a selected region of (h) the (1 1 1) peak marginally moving to lower angle for all catalysts and (i) the (3 1 1) reflection of $Co_3O_4$ at $2\theta = 37.5^\circ$, seen for the physical mixture only.

tor. The reactions were conducted in a stainless steel, fixed bed continuous flow reactor. The catalysts were crushed and collected through 300–600 μm sieves to obtain granules. For each experiment, a desired volume (0.70, 0.35 and 0.175 mL) of the catalyst was diluted with carborundum granules (24-grit) to a volume of 3 mL. The catalyst was placed in the isothermal zone, near the centre of the reactor tube. Empty spaces on either side of the catalyst bed were filled with carborundum and the ends plugged with glass wool. Prior to each reaction, the catalyst was pre-treated in situ in air flow at 150 °C for 4 h and then cooled to room temperature under nitrogen flow. For both total CO oxidation and PROX, the total flow rate was fixed at 140 mL/min while the mass of the catalyst was varied between 0.3 and 1.2 g to achieve gas hourly space velocities (GHSV) ranging from 12 000 to 48 000 $h^{-1}$. The catalytic behaviour of the catalysts was compared under different reaction feed compositions (provided in Table S1). For total CO oxidation, the feed composition was composed of 1 vol% CO and varied amounts of $O_2$; viz. 0.5, 1 and 2 vol%, corresponding to the λ values of 1, 2 and 4 respectively. In all experiments, $N_2$ was used as a balance gas. The factor λ is defined as the amount $O_2$ in the experiment relative to CO:

$$\lambda = \frac{2[O_2]_{in}}{[CO]_{in}} \quad (1)$$

In the case of PROX experiments, 50 vol% $H_2$ was included in the feed that was used for total CO oxidation. In addition, PROX experiments were also conducted in the presence of 7 vol% $H_2O$ and 15 vol% $CO_2$. Water was introduced by passing the dry gas through a bubbler kept at 38 °C. The stability of the catalysts was evaluated at 180 °C by performing PROX experiments as a function of time-on-stream (24 h). The time-on-stream studies were conducted by employing a reformate of 1 vol% CO, 1 vol% $O_2$, 50 vol% $H_2$ and 48 vol% $N_2$. A GHSV of 48000 $h^{-1}$ was used for all catalysts except for $Ce_{0.90}Co_{0.10}O_{2-\delta}$ where 12000 $h^{-1}$ was used to obtain comparable CO conversion. The effluent gases were analyzed using a three channel online Varian CP-4900 micro-GC, each channel equipped with a thermal conductivity detector (TCD). The GC has columns of Mol Sieve 5A and CP-Sil5CB with a 1.0 μL back-flushing system. The percentage of the converted CO and the $O_2$ selectivity to $CO_2$ were calculated using Eq. (2) and (3), respectively. The oxygen conversion was calculated using Eq. (4).

$$\text{COconversion}\,(X_{co}) = \frac{([CO]_{in}\text{-}[CO]_{out})}{[CO]_{in}} \times 100 \quad (2)$$

$$O_2\text{Selectivity to}\,CO_2\,\left(S_{CO_2}\right) = \frac{[CO]_{in}\text{-}[CO]_{out}}{2([O_2]_{in}\text{-}[O_2]_{out})} \times 100 \quad (3)$$

$$O_2\text{conversion}\,\left(X_{O_2}\right) = \frac{([O_2]_{in}\text{-}[O_2]_{out})}{[O_2]_{in}} \times 100 \quad (4)$$

In some instances, the activities are expressed in terms of specific rates (r), determined using Eq. (5), where $X_{CO}$ stands for CO conversion, $F_{CO}$ is the molar flow rate of CO (mol/s) and $m_{cat}$ (g) is the mass of the catalyst.

$$r = \frac{X_{CO} \times F_{CO}}{m_{cat}} \quad (5)$$

## 3. Results and discussion

### 3.1. Structural and morphology studies

The XRD diffractograms of $Ce_{0.90}Co_{0.10}O_{2-\delta}$, together with those of the copper containing analogues, $Ce_{0.90}Cu_xCo_{0.10}O_{2-\delta}$ (where $x = 0.01$, 0.03 and 0.05), are shown in Fig. 1. The XRD profiles of all catalysts show diffraction peaks that can be indexed to the fluorite structure of $CeO_2$. No $Co_3O_4$ diffraction peaks are identified in the X-ray diffractograms, except for those of $Ce_{0.87}Cu_{0.03}Co_{0.10}O_{2-\delta}$ and $Ce_{0.85}Cu_{0.05}Co_{0.10}O_{2-\delta}$, which showed a small metal oxide peak at 37.5°. This peak is characteristic of the (311) reflection of the $Co_3O_4$ spinel structure [41]. When the pure $Co_3O_4$ is predominantly on the surface of ceria, as seen from the XRD profiles of the physical mixture (10% $Co_3O_4/CeO_2$), it could unambiguously be detected (Fig. 1(i)). On the other hand, the diffraction peaks corresponding to CuO were not observed. The absence of these diffraction peaks suggests that copper ions have been successfully incorporated into the $CeO_2$ lattice. However, the existence of CuO finely dispersed on the surface and not detected by XRD is possible. In the past, it has been demonstrated that the incorporation of cobalt ions into ceria is difficult at atomic loadings exceeding 10%, $Ce_{1-x}Co_xO_{2-\delta}$ ($x > 0.1$) [39]. The same phenomenon may

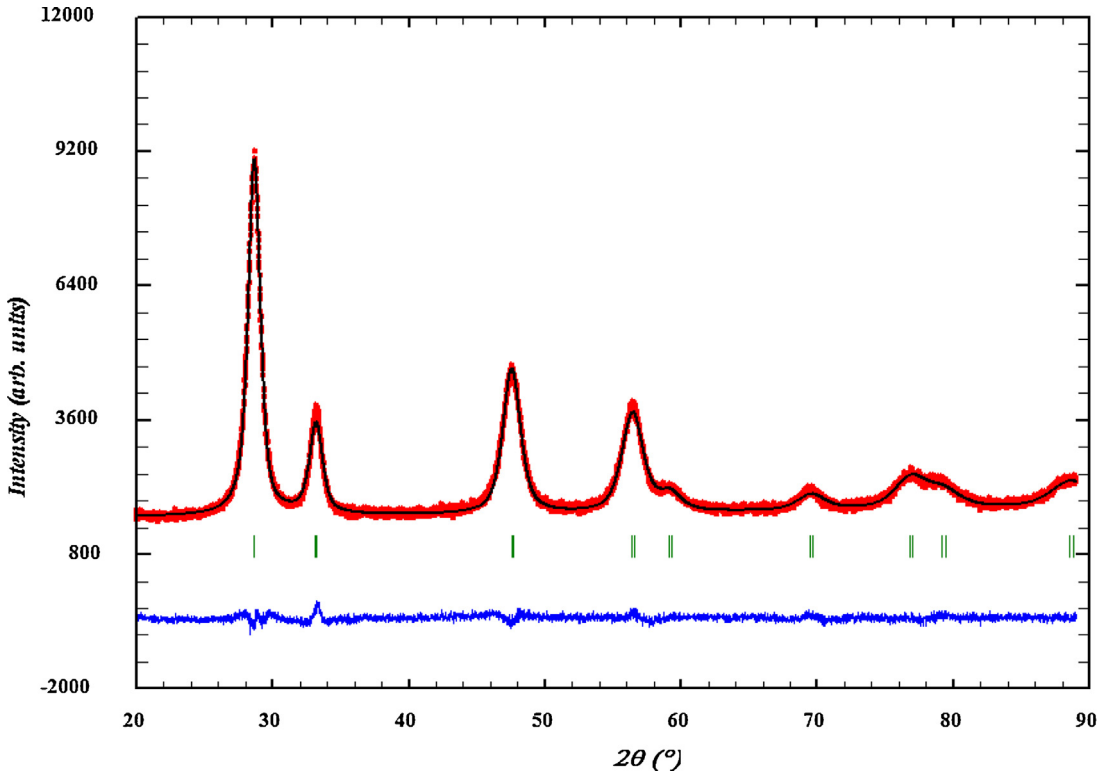


**Fig. 2.** Rietveld-refined XRD pattern of $Ce_{0.87}Cu_{0.03}Co_{0.1}O_{2-\delta}$.

apply with the $Ce_{0.87}Cu_{0.03}Co_{0.10}O_{2-\delta}$ and $Ce_{0.85}Cu_{0.05}Co_{0.10}O_{2-\delta}$ catalysts. All prepared ceria-based materials have broad diffraction peaks, indicative of the existence of small crystallites. Upon the incorporation of foreign metal ions into the ceria matrix, the diffraction lines slightly shifted to higher 2Θ values, which correspond to a slight decrease in the lattice constants. In the inset of Fig 1, it is shown that the (1 1 1) peak marginally moves when foreign metals are incorporated into the $CeO_2$ structure. This observation is in good agreement with the lattice parameters obtained from Rietveld analysis. A small decrease in lattice constant can also be associated with an increase in crystal size, as a consequence of size effects [42–45]. A typical Rietveld-refined XRD pattern is shown for $Ce_{0.89}Cu_{0.03}Co_{0.10}O_{2-\delta}$ in Fig. 2 and the other catalysts' Rietveld-refined patterns are provided in Fig. S1. The lattice parameter, $R_f$, $R_{bragg}$ and $\chi^2$ obtained from Rietveld refinement are summarized in Table 1. Except for $Ce_{0.85}Cu_{0.05}Co_{0.10}O_{2-\delta}$, all difference plots show a good fit, with no surface oxides. This suggests the formation of solid-solution materials. The observed, modelled and the difference (between observed and modelled) XRD patterns are represented in red, black and blue in the refined patterns.

Theoretically, the incorporation of dopant ions with smaller ionic radii in the $Ce^{4+}$ (0.97 Å) site are expected to be accompanied by a decrease in lattice parameter. Accordingly, substituted ceria materials, doped with $Co^{3+}$(0.63 Å) and/or $Cu^{2+}$(0.73 Å), show this value as being slightly lower than that of pure ceria (5.4221 Å) (39),

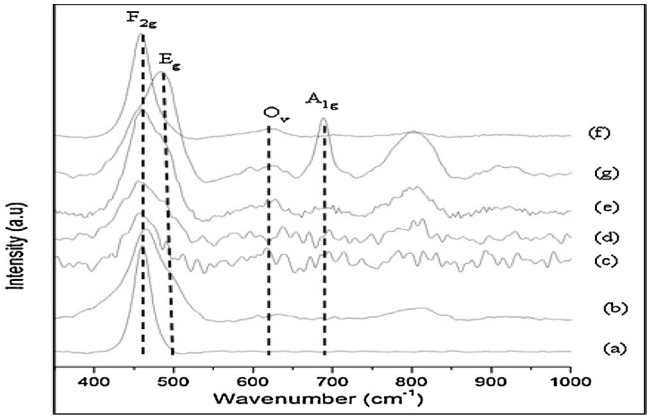


**Fig. 3.** Raman spectra of the prepared (a) $CeO_2$, (b) $Ce_{0.9}Co_{0.10}O_{2-\delta}$, (c) $Ce_{0.89}Cu_{0.01}Co_{0.10}O_{2-\delta}$, (d) $Ce_{0.87}Cu_{0.03}Co_{0.10}O_{2-\delta}$, (e) $Ce_{0.85}Cu_{0.05}Co_{0.10}O_{2-\delta}$, (f) $Ce_{0.95}Cu_{0.05}O_{2-\delta}$ and (g) $Co_3O_4$.

**Table 1**
Structural parameters of investigated catalysts obtained from XRD profiles.

| Catalyst | Lattice parameter a (Å) | Structure factor ($R_f$) | Bragg factor ($R_B$) | $\chi^2$ | Lattice strain ($10^{-3}$) | Crystallite size (nm) | d-spacing (nm)[a] |
|---|---|---|---|---|---|---|---|
| $CeO_2$ | 5.4221 | 1.95 | 3.06 | 1.24 | 1.10 | 8 | 0.307 |
| $Ce_{0.90}Co_{0.10}O_{2-\delta}$ | 5.4057 | 0.68 | 1.00 | 1.48 | 3.90 | 9 | 0.308 (0.31) |
| $Ce_{0.89}Co_{0.10}$ $Cu_{0.01}O_{2-\delta}$ | 5.4225 | 0.98 | 1.60 | 1.77 | 4.60 | 13 | 0.308 (0.33) |
| $Ce_{0.87}Co_{0.10}$ $Cu_{0.03}O_{2-\delta}$ | 5.4060 | 1.17 | 1.66 | 1.83 | 4.10 | 10 | 0.308 (0.33) |
| $Ce_{0.85}Co_{0.10}$ $Cu_{0.05}O_{2-\delta}$ | 5.4068 | 1.25 | 1.72 | 1.69 | 3.60 | 10 | 0.308 (0.34) |
| $Ce_{0.95}Cu_{0.05}O_{2-\delta}$ | 5.4185 | 1.12 | 1.76 | 1.87 | 3.80 | 13 | 0.308 (0.30) |

[a] Values show in parenthesis were estimated from HR-TEM.

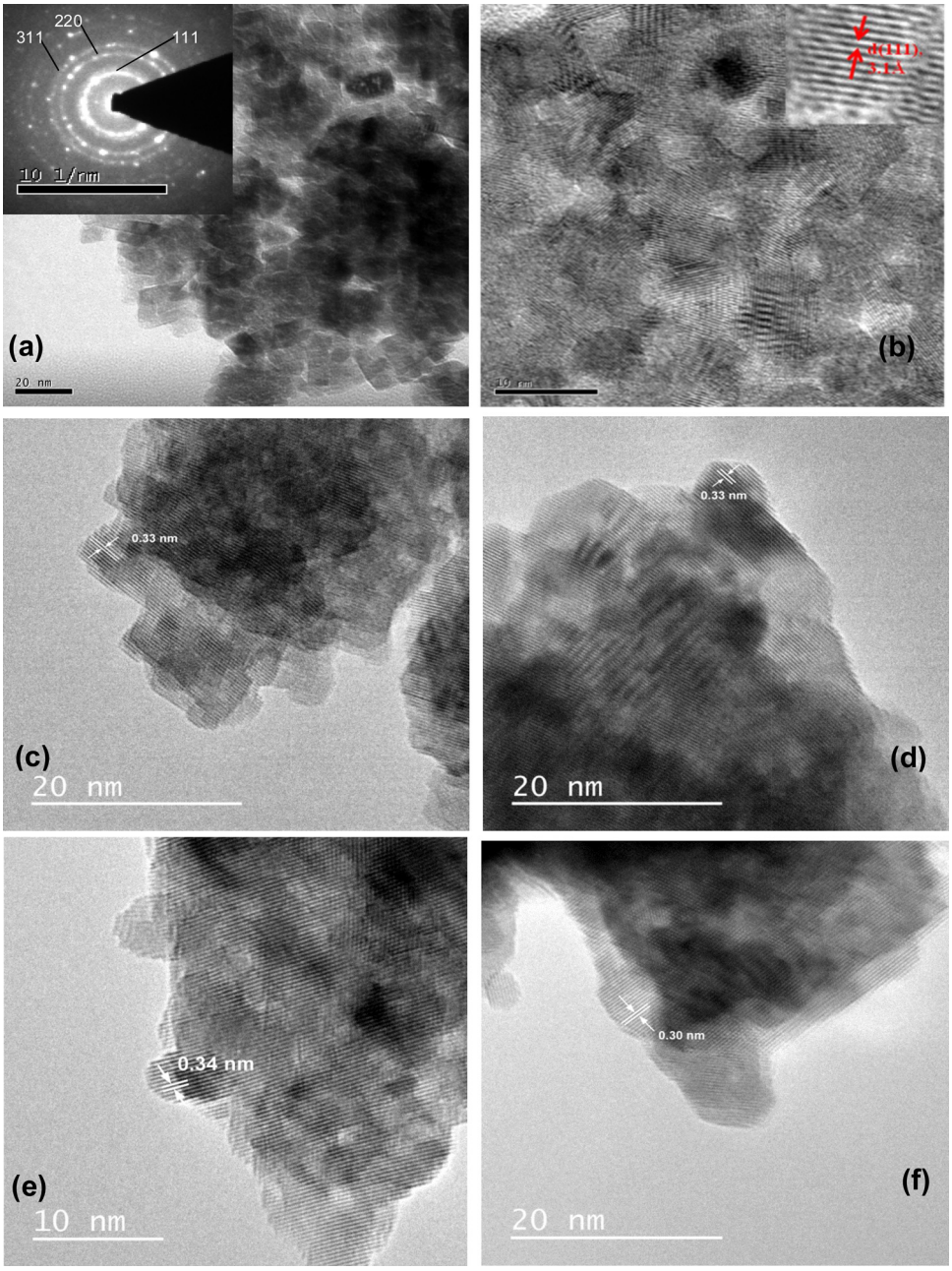


**Fig. 4.** (a) Bright field image and selected area electron diffraction of $Ce_{0.90}Co_{0.10}O_{2-\delta}$. HR-TEM images of (b) $Ce_{0.90}Co_{0.10}O_{2-\delta}$, (c) $Ce_{0.89}Cu_{0.01}Co_{0.10}O_{2-\delta}$, (d) $Ce_{0.87}Cu_{0.03}Co_{0.10}O_{2-\delta}$, (e) $Ce_{0.85}Cu_{0.05}Co_{0.10}O_{2-\delta}$ and (f) $Ce_{0.95}Cu_{0.05}O_{2-\delta}$.

except for $Ce_{0.89}Cu_{0.01}Co_{0.10}O_{2-\delta}$. In $Ce_{0.89}Cu_{0.01}Co_{0.10}O_{2-\delta}$, there is a slightly increase in the lattice parameter. This trend has been observed in cases in which the solid-solution materials have a high concentration of $Ce^{3+}$ species [46]. Therefore, this change may be as a result of counteractive contributions induced by the incorporation of foreign metal ions and the presence of defects of $Ce^{3+}$ ions. As observed with the peak shifts, simultaneous introduction of both metal ions did not lead to significant changes in the lattice parameter. Perhaps, further changes are limited because of the difficulty of incorporating the entirety of both dopant ions at loadings above 10%, as seen for $Ce_{0.87}Cu_{0.03}Co_{0.10}O_{2-\delta}$ and $Ce_{0.85}Cu_{0.05}Co_{0.10}O_{2-\delta}$.

Williamson-Hall (W-H) plots and Eq. (6) were used to determine the lattice strain ($\epsilon$) and crystallite size ($D$) for each of the prepared samples (W-H plots are provided in Fig. S2). A linear fit is drawn with $\beta_{hkl}\cos\theta$ on the $y$-axis and $4\epsilon\sin\theta$ along the $x$-axis. Pure ceria was found to have the least lattice strain. The lattice strain increases upon the introduction of dopants and it is at its maximum for samples that showed no peaks corresponding to the surface oxides. It is possible that the strain observed for $Ce_{0.85}Cu_{0.05}Co_{0.10}O_{2-\delta}$ is predominantly influenced by the insertion of $Cu^{2+}$, as it is comparable with that of $Ce_{0.95}Cu_{0.05}O_{2-\delta}$.

$$\beta_{hkl}\cos\theta = \frac{K\lambda}{D} + 4\epsilon\sin\theta \quad (6)$$

The average crystallite sizes of all the prepared materials are below 15 nm (Table 1).

The structural properties of ceria-based catalysts were also studied by Raman spectroscopy, employing the laser wavelength of 514 nm. Fig. 3 depicts the Raman spectra of the metal ion substituted ceria materials together with those of pure $CeO_2$ and $Co_3O_4$. All ceria based materials show an intense main peak at $\approx$460 $cm^{-1}$ which is associated with the triply degenerate ($F_{2g}$)

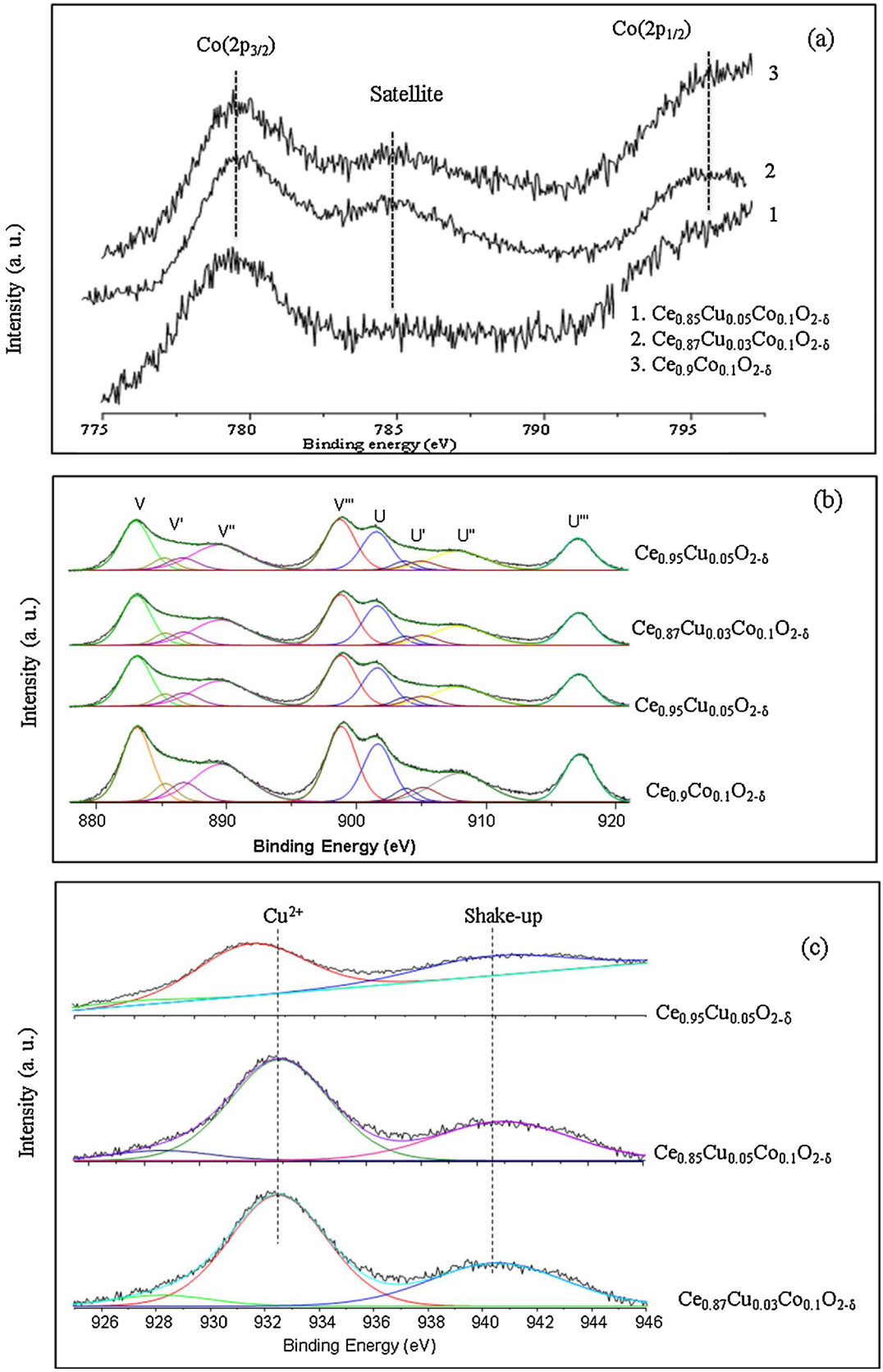


**Fig. 5.** XP spectra of the catalysts: (a) Co(2p), (b) Ce(3d) and (c) Cu(2p).

phonon mode of the cubic fluorite structure [32]. These observations are in agreement with the XRD results, indicating that the fluorite structure is retained upon metal substitution. For substituted ceria samples, an additional broad band is observed between 550 and 650 $cm^{-1}$. Generally, this peak is ascribed to the presence of oxygen vacancy defects ($O_v$) which are generated to compensate

for charge imbalance after the incorporation of dopants with lower valence [12]. In the case of $Ce_{0.9}Co_{0.10}O_{2-\delta}$, $Ce_{0.85}Cu_{0.05}Co_{0.10}O_{2-\delta}$ and $Ce_{0.95}Cu_{0.05}O_{2-\delta}$, the $O_v$ band was relatively more intense compared to other samples, indicating the presence of substantial oxygen vacancies. The absence of the $O_v$ band in pure $CeO_2$ suggests that the vacancies present in the doped materials are not mainly intrinsic ones due to the presence of $Ce^{3+}$ [47]. Instead, they are mostly extrinsic vacancies as a consequence of incorporating foreign metal ions in the fluorite lattice [48]. Notably, the $F_{2g}$ bands of substituted ceria materials have an increased width relative to pure ceria. This phenomenon has been associated with the manifestation of inhomogeneous strain, as a result of present oxygen vacancy defects due to metal insertion into the fluorite lattice [49].

The HR-TEM and bright-field images of the catalysts are presented in Fig. 4. The morphologies of the catalysts seem to be comparable, regardless of further doping with Cu. The images show the presence of agglomerates of near-spherical nanoparticles. From image analysis, the materials are composed of nanoparticles of relatively uniform size (6–16 nm) which is comparable to the crystallite size deduced from XRD data (Table 1). In general, the selected area diffraction of images (Fig. 4(a)) show a ring pattern that can be indexed to the fluorite structure and is in agreement with XRD data. Moreover, the HR-TEM images of all the catalysts show lattice fringes with interplanar distances between 0.30 to 0.34 nm, corresponding to the (1 1 1) facets of fluorite-structured solid-solutions [12]. The FEG-SEM micrographs reveal that all catalysts possess microspheres which are made up of uniform small nanocrystals. The corresponding EDS results confirmed the presence of Ce, Co and Cu in the catalysts. As further doping does not translate to morphological changes, different catalytic behaviour may not be linked to the differences in morphology. The precise compositions of the catalysts were further established on the basis ICP-OES analysis. The FEG-SEM microscopic images and ICP OES results of all the samples are provided in Fig. S3 and Table S2 respectively.

### 3.2. Textural studies

The study of the textural properties of the catalysts suggests that the materials are mesoporous with some microporosity features. The nitrogen adsorption/desorption isotherms reveal a sharp increase in adsorption at high relative pressures, which suggests the filling of the mesopores [50]. The pore size distribution curves show a peak in the range of 2.5–5 nm, confirming the existence of mesoporous structures. As anticipated, the surface areas and pore volumes of ceria decrease upon the insertion of foreign metals into the matrix structure. The surface areas of the studied solid-solution materials range from 14 to 27 $m^2/g$, with $Ce_{0.90}Co_{0.10}O_{2-\delta}$ having the largest and $Ce_{0.89}Cu_{0.01}Co_{0.10}O_{2-\delta}$ having the smallest surface area. Nitrogen adsorption/desorption isotherms and pore size distribution curves and analysed textural properties of all the catalysts are provided in Fig. S4 and Table S2 respectively.

### 3.3. Electronic and redox properties

In order to investigate the redox properties of the catalysts, $H_2$-TPR measurements of the catalysts were conducted. Pure ceria showed no $H_2$ consumption up to 400 °C, indicating that it could not be reduced in this temperature window under current experimental conditions. A comparison of the $H_2$-TPR profiles of $Ce_{0.90}Co_{0.10}O_{2-\delta}$, $Ce_{0.89}Cu_{0.01}Co_{0.10}O_{2-\delta}$, $Ce_{0.87}Cu_{0.03}Co_{0.10}O_{2-\delta}$, $Ce_{0.85}Cu_{0.05}Co_{0.10}O_{2-\delta}$ and $Ce_{0.95}Cu_{0.05}O_{2-\delta}$ is provided in Fig. S5. Regarding the reduction profile of $Ce_{0.90}Co_{0.10}O_{2-\delta}$, two reduction peaks can be seen at 280 °C and 343 °C. This suggests that the reduction is a step-wise process, where the former peak is due to the reduction of $Co^{3+}$ to $Co^{2+}$ and the latter can be attributed to the reduction of $Co^{2+}$ to $Co^0$. This reduction pattern is well known

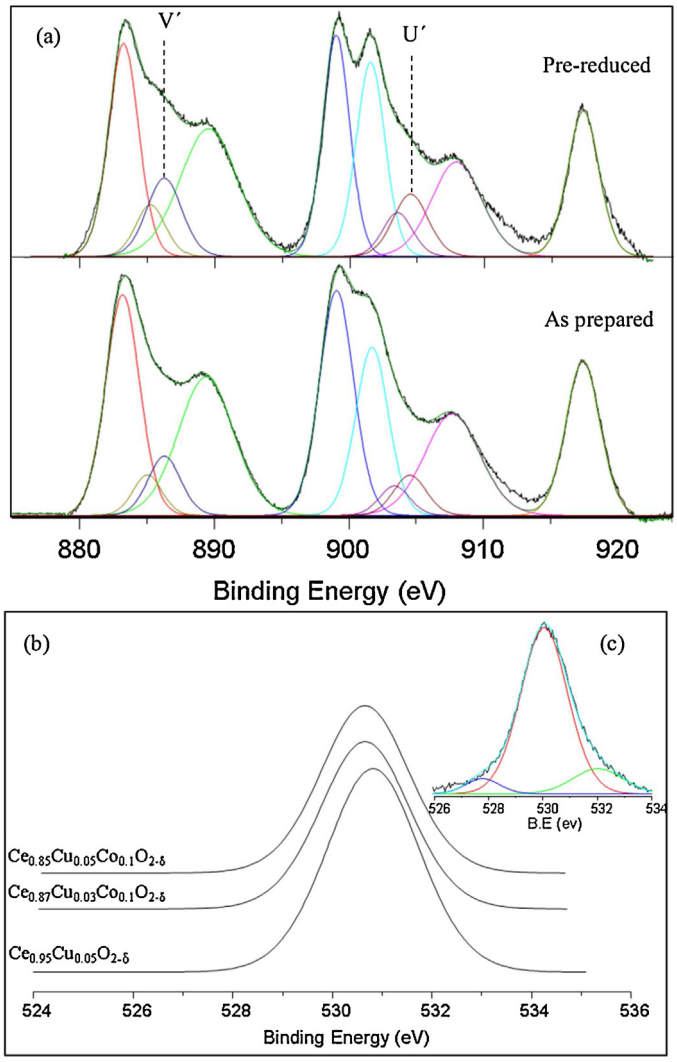


**Fig. 6.** Ce(3d) XP spectra of (a) pre-reduced and as-prepared catalyst. (b) and (c) O(1s) XP spectra of the catalysts.

for pure $Co_3O_4$ [31]. In comparison with the reported reduction peaks for pure $Co_3O_4$, the reduction peaks for the Ce–Co catalysts are lower, suggesting an improved reducibility of cobalt ions as reported elsewhere [46]. In the case of the $Ce_{0.95}Cu_{0.05}O_{2-\delta}$ sample, two overlapping reduction peaks are observed at 186 °C and 211 °C. The mentioned two peaks profile is typical for Cu–Ce samples [51–53]. It has been related to the reduction of two different types of copper oxide entities differing in their degree of interaction with the support. The low temperature peak would correspond to smaller copper oxide particles subjected to a stronger interaction with the support which would favour their reduction, while the high temperature peak would correspond to larger copper oxide particles [51,54]. $Ce_{0.89}Cu_{0.01}Co_{0.10}O_{2-\delta}$, $Ce_{0.87}Cu_{0.03}Co_{0.10}O_{2-\delta}$ and $Ce_{0.85}Cu_{0.05}Co_{0.10}O_{2-\delta}$ show three coinciding peaks located at reduction temperatures lower than those observed in the profile of $Ce_{0.90}Co_{0.10}O_{2-\delta}$. Since the hydrogen consumption related to these peaks is higher than the theoretical consumption due to the reduction of cobalt oxide species to metallic cobalt, the overlapping peaks also represent the reduction of copper ions to $Cu^0$. The incorporation of $Cu^{2+}$ ions into the Co-containing catalyst stimulates the reduction of Co ions to a certain degree, depending on the Cu loading. By comparison, temperatures corresponding to cobalt oxide reduction steps decrease in the order of $Ce_{0.90}Co_{0.10}O_{2-\delta} \square Ce_{0.89}Cu_{0.01}Co_{0.10}O_{2-\delta} \approx Ce_{0.87}Cu_{0.03}Co_{0.10}O_{2-\delta}$

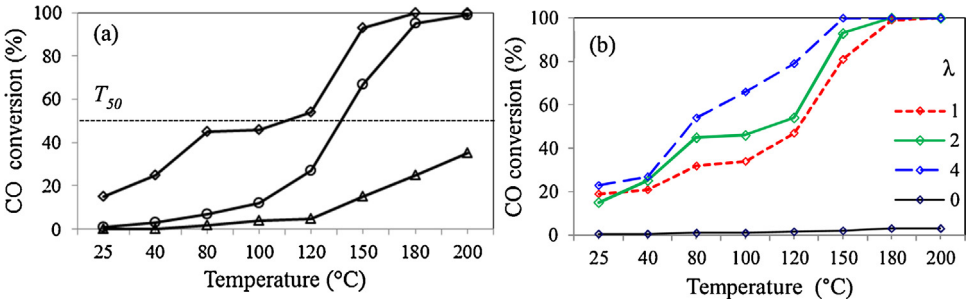


**Fig. 7.** (a) CO conversion as a function of temperature over Δ $CeO_2$, ○ 10%$Co_3O_4/CeO_2$ and ◊ $Ce_{0.90}Co_{0.10}O_{2-\delta}$ in TOX reaction (Conditions: λ = 2, GHSV = 12000 $h^{-1}$). (b) CO conversion at different $O_2$/CO ratios over $Ce_{0.90}Co_{0.10}O_{2-\delta}$ in TOX reaction.

□$Ce_{0.85}Cu_{0.05}Co_{0.10}O_{2-\delta}$ ≈$Ce_{0.95}Cu_{0.05}O_{2-\delta}$. Based on the amount of total hydrogen consumption, calculated up to the temperature of 400 °C, the oxygen storage capacity was estimated [55,56] to be 78, 196, 210, 257 and 442 μmol/g for $Ce_{0.9}Co_{0.10}O_{2-\delta}$, $Ce_{0.89}Cu_{0.01}Co_{0.10}O_{2-\delta}$, $Ce_{0.95}Cu_{0.05}O_{2-\delta}$, $Ce_{0.87}Cu_{0.03}Co_{0.10}O_{2-\delta}$ and $Ce_{0.85}Cu_{0.05}Co_{0.10}O_{2-\delta}$, respectively. Notably, it increases with the increase of the Cu atomic loading in the Co-containing samples as a consequence of additional reduction of incorporated Cu ions [13]. Among all the studied catalyst formulations, $Ce_{0.95}Cu_{0.05}O_{2-\delta}$ is the most easily reducible, with the first reduction peak located at 186 °C. This is due to the strong interaction between cerium and copper ions, which is even more enhanced in the absence of cobalt ions.

XPS was used to establish the electronic properties of Co, Cu and Ce in the prepared solid-solution materials. Fig. 5(a) shows the Co (2p) XP spectra of Co-containing catalysts. For all samples, the main peak at the binding energy of 779 eV is characteristic of Co ($2p_{3/2}$), while the shoulder peak at 795 eV can be attributed to Co ($2p_{1/2}$). In the case of $Ce_{0.90}Co_{0.10}O_{2-\delta}$, the satellite peak can be seen as a broad peak at ~5.5 eV above the main peak. Overall, the spectra unambiguously confirm the presence of $Co^{2+}$ in the high spin state [57,58]. However, the existence of $Co^{3+}$ species cannot completely be ruled out since the Co($2p_{3/2}$) binding energies of $Co^{2+}$ appear between 780 and 782 eV, which is relatively close to the region (779–782 eV) where those of $Co^{3+}$ emerge [58]. Thus, it is often difficult to distinguish the two oxidation states based on their binding energies.

The Ce(3d) and Cu(2p) core level regions of the selected ceria-based catalysts are depicted in Fig. 5(b) and (c), respectively. The Ce (3d) XPS spectra of all studied catalysts show eight peaks associated with the pairs of spin-orbit doublets. The peaks labeled U (U-U‴) and those assigned as V (V-V‴) are related to the $3d_{3/2}$ and $3d_{5/2}$ spin-orbit components, respectively. Due to the closeness of U′ and V′ peaks to the main neighboring peaks (U and V), the former peaks are not well resolved. The couple (U′, V′) is characteristic of the $Ce^{3+}$ species and the rest of the peaks correspond to the $Ce^{4+}$ state as in $CeO_2$. The existence of the $Ce^{3+}$ species was further confirmed by recording the XPS of a pre-reduced $Ce_{0.87}Cu_{0.03}Co_{0.1}O_{2-\delta}$ sample. For a reduced sample, the crescents formed between (V, V″) and (U U″) are not well-defined as a consequence of increased $Ce^{3+}$ components, V′ and U′ (Fig. 6(a)). Although all catalysts contain Ce predominantly in the +4 oxidation state, some degree of $Ce^{3+}$ species is also present.

The Cu-containing catalysts ($Ce_{0.87}Cu_{0.03}Co_{0.10}O_{2-\delta}$, $Ce_{0.85}Cu_{0.05}Co_{0.10}O_{2-\delta}$ and $Ce_{0.95}Cu_{0.05}O_{2-\delta}$) show weak shake-up and Cu ($2p_{3/2}$) peaks at the binding energies of 940.5 eV and 932.5 eV, respectively. The weak intensity of the shake-up peak has been associated with the presence of reduced copper species, particularly $Cu^+$, in CuO–$CeO_2$ catalysts [6,19]. The formation of $Cu^+$ entities can be explained in two ways. Taking into account the similarity of the $Ce^{4+}$ (0.97 Å) and $Cu^+$ (0.96 Å) ionic radii, $Cu^+$ formation might be induced during substitution [6]. On the other hand, the copper species, in CuO–$CeO_2$, may be reduced during XPS measurements due to the desorption of surface oxygen under vacuum [19]. Summarily, the observations reported here suggest the presence of $Cu^{2+}$ and $Cu^+$ species and are in good agreement with the TPR profiles. The O(1s) XP spectra of the catalysts with different Cu loadings were also examined (Fig. 6(b)). The peaks that are associated with the lattice oxygen of $Ce_{0.87}Cu_{0.03}Co_{0.10}O_{2-\delta}$ and $Ce_{0.85}Cu_{0.05}Co_{0.10}O_{2-\delta}$ are centered at a binding energy of nearly 530.8 eV. In the case of $Ce_{0.95}Cu_{0.05}O_{2-\delta}$, the lattice oxygen peak appears at a slightly higher binding energy and is accompanied by a shoulder peak at 531.5 eV. The latter peak can be seen distinctly on a fitted spectrum shown in Fig. 6(c). Although the exact origin of this peak has been disputed, it is often attributed to the surface oxygen and linked to the outstanding oxidative catalysis demonstrated by $CeO_2$-based formulations [59].

### 3.4. Catalytic studies

#### 3.4.1. Total and preferential CO oxidation over $Ce_{90}Co_{10}O_{2-\delta}$

The catalytic activity of the catalysts was investigated in total CO oxidation in the temperature range of 25 °C–200 °C, by employing different feed-stream compositions. Bare ceria was also studied in order to emphasize the effect of incorporating cobalt ions into the ceria lattice. Fig. 7(a) shows the typical light-off curves of the total CO oxidation reaction over non-substituted $CeO_2$, $Ce_{0.90}Co_{0.10}O_{2-\delta}$ and 10 wt% $Co_3O_4/CeO_2$. As seen for the Co-containing solid-solution catalyst, CO conversion increases with temperature until complete conversion is reached at temperatures above 150 °C (depending on the $O_2$/CO ratio and/or GHSV used). The temperatures for a CO conversion of 50% are marked with a dotted line on the graph. It is observed that neat ceria shows no significant CO conversion until higher temperatures are reached (150–200 °C). Since pure $CeO_2$ and $Ce_{0.90}Co_{0.10}O_{2-\delta}$ were prepared under the same combustion conditions, the better catalytic performance demonstrated by cobalt substituted ceria suggests that the Co ions in the ceria lattice are involved in the promotion of CO activation during the TOX reaction. Moreover, the solid solution catalyst displays superior activity to the physical mixture material (10 wt% $Co_3O_4/CeO_2$). The enhanced catalytic activity over the Ce–Co catalyst is due to the stronger interaction of cobalt with ceria ions. It is envisaged that such synergism is limited in 10 wt% $Co_3O_4/CeO_2$. The catalytic profile of $Ce_{0.90}Co_{0.10}O_{2-\delta}$ also appears to be outperforming some of the results reported for 10 wt% $Co_3O_4/CeO_2$ [60] and $Ce_{0.90}MnO_{0.10}O_2$ [35] composites, which showed complete CO conversion at 420 °C and a maximum of 90% CO conversion at 225 °C, respectively.

In the feed composition with the $O_2$ proportion (λ = 1) corresponding to the stoichiometric amount needed to convert all the CO (1 vol%), it would be expected that $O_2$ gets depleted at the point of complete CO oxidation. Notably, although the $O_2$ conversion is

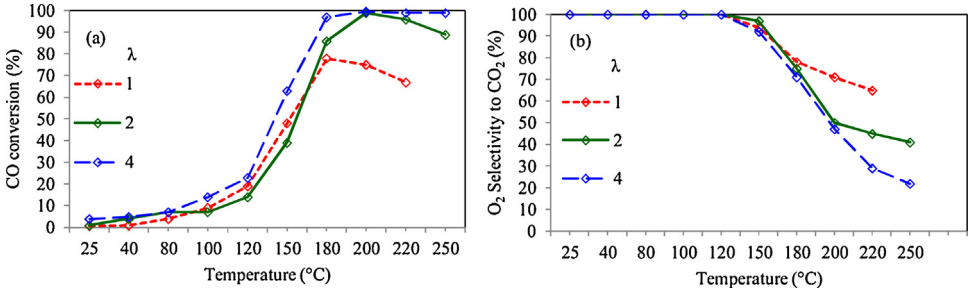


**Fig. 8.** (a) CO conversion and (b) selectivity as a function of temperature at different $O_2$/CO ratios over $Ce_{0.90}Co_{0.10}O_{2-\delta}$ in PROX reaction. Experimental conditions: λ = 1 to 4, GHSV = 12000 $h^{-1}$.

proportional to CO conversion, it was in the range of 91–93 % at the point of complete CO conversion, during the sampling time of 30 min. With this in mind, TOX experiments were also conducted in the absence of feed $O_2$ (λ = 0) to examine the possibility of the involvement of the lattice oxygen in CO oxidation. In the absence of feed oxygen, CO does get converted to $CO_2$ although the CO conversions are low (Fig. 7(b)). This observation suggests that CO gets oxidized through direct reaction with the activated lattice oxygen. However, this conversion is marginal. Such a catalytic property is consistent with a dual site mechanism that has been proposed for the oxidation of *n* -octane over a $Ce_{0.90}Co_{0.10}O_{2-\delta}$ and CO oxidation over a $Ce_{1-x}Pt_xO_2$ catalyst [37,61]. The high activity of the cobalt substituted ceria catalyst in CO oxidation can be explained based on a well-known phenomenon of the development of oxide ion vacancies when transition metals are incorporated into a ceria or titania matrix [12]. During CO oxidation over $Ce_{0.90}Co_{0.10}O_{2-\delta}$, CO adsorbs on $Co^{2+}$ ions and feed $O_2$ occupies oxide ion vacant sites generated upon the formation of a solid-solution. The mobility of lattice oxygen is aided by the redox behavior between the two metal ions. After the formation of $CO_2$, the feed oxygen fills the vacant sites for the next catalytic cycle. Therefore, CO oxidation over cobalt substituted ceria catalysts follows a Mars-van Krevelen (MvK) type mechanism, which is a widely accepted pathway for ceria-based oxide catalysts [62]. The reaction progression relies on a continuous supply of feed $O_2$ as inherent oxygen contributes marginally and would eventually get depleted.

As shown in Fig. 7(b), the minimum temperature for complete CO oxidation decreases with increasing the proportion of $O_2$ in the feed: 180 °C for λ = 1 or 2 and 150 °C for λ = 4. As expected when the GHSV is lowered, complete CO oxidation is reached at even lower temperatures: 150 °C for 12000 $h^{-1}$, if the λ factor is kept at 4. This trend can be attributed to the different residence times of the reactants.

Preferential CO oxidation was studied under the same conditions as those employed for total CO oxidation, but with high hydrogen content (50 vol%). Similarly to total CO oxidation, CO conversion increases with increasing temperature (Fig. 8). It must be underlined that no significant CO and $O_2$ conversions (≤10%) can be observed until 80 °C, regardless of the GHSV and/or $O_2$/CO ratio used. Regardless of the $O_2$/CO ratio and/or GHSV employed, the catalyst shows a stable selectivity of $O_2$ to $CO_2$, between 98 and 100 %, at reaction temperatures below 150 °C. This, however, does not suggest that the catalyst selectively adsorbs CO in a low temperature region. Unlike noble metal catalytic systems [9], most transition metal oxides are known to adsorb both CO and $H_2$ non-competitively [63]. Nonetheless, $H_2$ oxidation can only happen at high temperatures due to the higher required activation energy for this reaction [31]. Consequently, Fig. 8(b) confirms that the selectivity is not sensitive to the $O_2$/CO ratio at temperatures below 200 °C, even in the presence of excess $O_2$. For metal oxide catalysed PROX reactions, such a reaction profile is consistent with the operation of the Mars-van Krevelen pathway [24]. Although supported $Co_3O_4$ catalysts [64] and other analogous catalysts [22] have been reported to selectively oxidize CO to $CO_2$ in the presence of $H_2$, the maximum selectivity is not maintained for a wide temperature window. It is worth mentioning that well-known PROX catalysts start to experience a drop in selectivity at temperatures as low as 30 °C (for Au) and 100 °C (for Cu) [65]. In summary, at temperatures above 100 °C, the conversion increases at the given temperature with the decrease in GHSV: 12 000 (97%) >24 000 (85%) >48000 $h^{-1}$ (63%) at 180 °C. On the other hand, at temperatures beyond 150 °C, selectivity at given temperatures can be improved by increasing GHSV: 12 000 (71%) <24 000 (76%) <48 000 $h^{-1}$ (84%) at 180 °C (Fig. 9). Complete CO conversion and high selectivity by the studied catalyst, in PROX, can be achieved by manipulating GHSV and $O_2$ concentration.

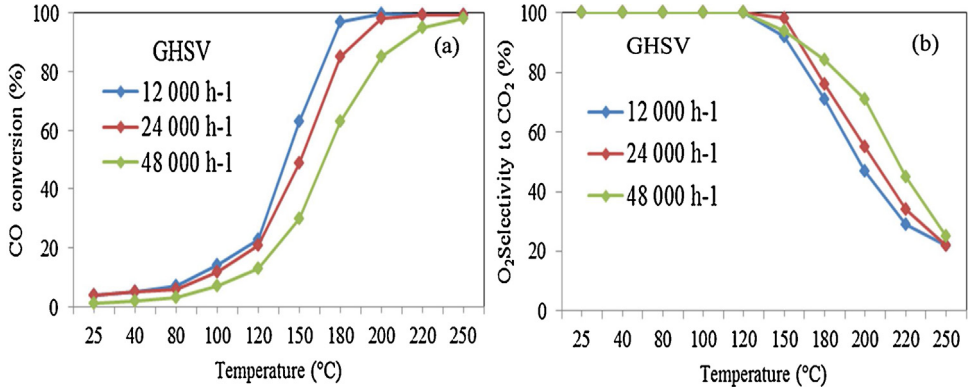


**Fig. 9.** (a) CO conversion and (b) selectivity as a function of temperature at different GHSV (12000–48000 $h^{-1}$) over $Ce_{0.90}Co_{0.10}O_{2-\delta}$ in PROX reaction. Experimental conditions: λ = 4.

**Table 3**
PROX activity and selectivity of investigated catalysts under different gas mixtures.

| Catalyst | CO conversion and selectivity [a] | | | |
|---|---|---|---|---|
| | $H_2O/CO_2$-free | 15 vol% $CO_2$ | 7 vol% $H_2O$ | 15 vol% $CO_2$ and 7 vol% $H_2O$ |
| $Ce_{0.90}Co_{0.10}O_{2-\delta}$ | 90 (72) | 32 (80) | 50 (85) | 13 (77) |
| $Ce_{0.89}Co_{0.10}Cu_{0.01}O_{2-\delta}$ | 81 (82) | 62 (86) | 43 (95) | 18 (96) |
| $Ce_{0.87}Co_{0.10}Cu_{0.03}O_{2-\delta}$ | 92 (72) | 79 (80) | 52 (83) | 31 (92) |
| $Ce_{0.85}Co_{0.10}Cu_{0.05}O_{2-\delta}$ | 95 (63) | 90 (72) | 79 (80) | 36 (86) |
| $Ce_{0.95}Cu_{0.05}O_{2-\delta}$ | 96 (50) | 93 (56) | 95 (65) | 86 (75) |

[a] The values outside and inside brackets represent conversion and selectivity, respectively.

### 3.4.2. *The promotional effect of Cu on the TOX and PROX activity of $Ce_{0.90}Co_{0.10}O_{2-\delta}$*

The $CuO/CeO_2$ catalyst formulations are generally associated with improved oxygen mobility and optimized redox properties, which in turn promote oxidative catalysis [66]. In an attempt to improve the activity of $Ce_{0.90}Co_{0.10}O_{2-\delta}$ by possibly harnessing Ce–Co and Ce–Cu synergetic effects, Cu ion additives were incorporated to form bimetallic solid-solution catalysts, $Ce_{0.90-x}Cu_xCo_{0.10}O_{2-\delta}$ (where $x = 0$, 0.01, 0.03 and 0.05). Fig. 10 shows the CO conversion during the TOX reaction over $Ce_{0.90-x}Cu_xCo_{0.10}O_{2-\delta}$ catalysts with varied Cu content. As the Cu atomic loading increases from 0 to 3 at%, no significant improvement is observed. The temperatures for a CO conversion of 50% are almost the same for $Ce_{0.90}Co_{0.10}O_{2-\delta}$ and $Ce_{0.87}Cu_{0.03}Co_{0.10}O_{2-\delta}$. Notably, $Ce_{0.85}Cu_{0.05}Co_{0.10}O_{2-\delta}$ displays the best catalytic performance among the bimetallic systems, with the lowest temperatures for 50% and complete CO conversion. It is noteworthy that the activity of this catalyst has a parallel relationship with its $H_2$-TPR profile, which shows low temperature reduction. For a holistic evaluation, the catalytic activity of the catalyst that contains no cobalt ions, $Ce_{0.95}Cu_{0.05}O_{2-\delta}$, was also studied. Interestingly, this catalyst shows superior performance among all studied catalysts. This suggests that there is a close contact between Ce and Cu in the absence of cobalt. Since the XRD data confirmed the formation of a homogeneous solid-solution, it can be concluded that the interaction between the two ions is enhanced, as revealed by easy reducibility. Based on the temperature values corresponding to 50 and 100% CO conversions ($T_{50}$and $T_{100}$), the activity follows the order: $Ce_{0.95}Cu_{0.05}O_{2-\delta} > Ce_{0.85}Cu_{0.05}Co_{0.10}O_{2-\delta} > Ce_{0.9}Co_{0.10}O_{2-\delta} \approx Ce_{0.87}Cu_{0.03}Co_{0.10}O_{2-\delta} > Ce_{0.89}Cu_{0.01}Co_{0.10}O_{2-\delta}$.

The catalytic performance of the bimetallic materials and their respective monometallic catalysts was also studied under PROX reaction conditions. The CO conversion and $O_2$ selectivity, as a function of temperature, are shown in Fig. 11. As depicted in Fig. 11(a), $Ce_{0.90}Co_{0.10}O_{2-\delta}$ displays the lowest catalytic activity and has a $T_{50}$value that is higher than 150 °C. Incorporating Cu ion additives results in bimetallic catalysts with improved catalytic activity. The CO conversion increases substantially with Cu loading increments, from 0 to 5 at %, which is indicative of the promotional effect by Cu ions. Similarly to total CO oxidation, $Ce_{0.85}Cu_{0.05}Co_{0.10}O_{2-\delta}$ displays superior catalytic performance relative to the other bimetallic analogues. For this catalyst, $T_{50}$ and $T_{100}$ temperatures are lower than those of other $Ce_{0.90-x}Cu_xCo_{0.10}O_{2-\delta}$ catalysts and are very close to the values observed for $Ce_{0.95}Cu_{0.05}O_{2-\delta}$. As it can be seen from Fig. 11(b), all studied catalysts are highly selective for CO oxidation, showing no sign of $H_2$ oxidation at temperatures below 150 °C. Notably, methane formation was not observed in the studied reaction temperature window (25–250 °C) over the prepared catalysts. Methanation over related catalysts was reported to light-off above the temperature selected in the present report [67].

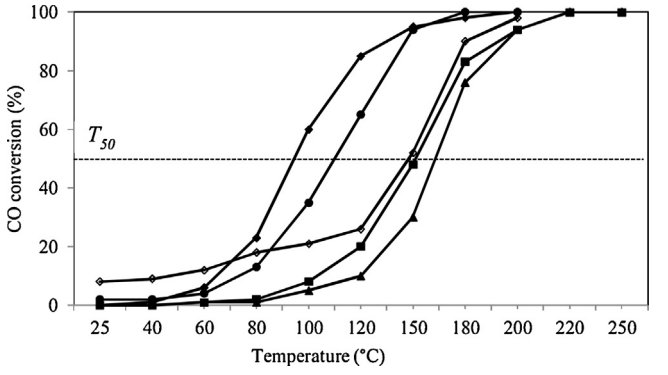


**Fig. 10.** CO conversion as a function of temperature over ceria-based catalysts in TOX reaction. ◊ = $Ce_{0.9}Co_{0.10}O_{2-\delta}$, ▲ = $Ce_{0.89}Cu_{0.01}Co_{0.10}O_{2-\delta}$, ■ = $Ce_{0.87}Cu_{0.03}Co_{0.10}O_{2-\delta}$, ● = $Ce_{0.85}Cu_{0.05}Co_{0.10}O_{2-\delta}$ and ♦ = $Ce_{0.95}Cu_{0.05}O_{2-\delta}$.Conditions: λ = 2, GHSV = 48000 $h^{-1}$.

Interestingly, the activity order of the catalysts in the $H_2$-rich environment ($Ce_{0.95}Cu_{0.05}O_{2-\delta} \approx Ce_{0.85}Cu_{0.05}Co_{0.10}O_{2-\delta} > Ce_{0.87}Cu_{0.03}Co_{0.10}O_{2-\delta} > Ce_{0.89}Cu_{0.01}Co_{0.10}O_{2-\delta} > Ce_{0.90}Co_{0.10}O_{2-\delta}$) is not similar to the trend observed for $H_2$-free experiments. To gain more understanding on the catalytic performance of the catalysts, the specific reaction rates were calculated at a reaction temperature of 150 °C, according to a reported method [7]. This reaction temperature is high enough to gain insight into the PROX reaction network. Since pure $CeO_2$ shows some minor activity at this temperature and above, the specific reaction rates are expressed as moles of CO converted per gram of the catalyst (not Co and/or Cu) and per second. Furthermore, the plots of specific rates with temperature were drawn using data points where CO conversion is below 30% (Fig. 12(A, B). The corresponding Arrhenius plots and activation energy values for TOX and PROX are shown in Fig. 12(C, D) and summarized in Table 2 respectively. For both TOX and PROX studies, all Cu-containing catalysts clearly do not show a decline in CO conversion in the presence of $H_2$, while the opposite is true for $Ce_{0.90}Co_{0.10}O_{2-\delta}$. Considering the 150 °C points, it is seen in Fig. 13, the activity of $Ce_{0.89}Cu_{0.01}Co_{0.10}O_{2-\delta}$ and $Ce_{0.87}Cu_{0.03}Co_{0.10}O_{2-\delta}$ is improved upon introducing $H_2$, with CO conversions increased from 30% to 49% and 48% to 72%, respectively. Accordingly, the specific reaction rates of these catalysts increase from $1.04 \times 10^{-4}$ to $1.70 \times 10^{-4}$ mol $g^{-1}$ $s^{-1}$ for the former and from $1.67 \times 10^{-4}$ to $2.50 \times 10^{-4}$ mol $g^{-1}$ $s^{-1}$ for the latter. In contrast, CO conversion over $Ce_{0.90}Co_{0.10}O_{2-\delta}$ decreases by half in the $H_2$-rich stream, with respective specific rates of $1.81 \times 10^{-4}$ and $9.03 \times 10^{-5}$ mol $g^{-1}$ $s^{-1}$ in TOX and PROX experiments. The performance of $Ce_{0.85}Cu_{0.05}Co_{0.10}O_{2-\delta}$ and $Ce_{0.95}Cu_{0.05}O_{2-\delta}$ appears comparable and unaffected by the absence or presence of $H_2$.

It is also shown that $Ce_{0.90}Co_{0.10}O_{2-\delta}$ maintains its oxygen selectivity to $CO_2$ at 100 % (Fig. 13) and the $O_2$ consumption does not increase in the presence of $H_2$. Instead the $O_2$ conversion decreases, which indicates that the decrease in CO conversion is not associated with $O_2$ consumption by the undesirable $H_2$ oxidation reaction. These results suggest that, over $Ce_{0.90}Co_{0.10}O_{2-\delta}$, the $H_2$ interacts with the same active sites where CO oxidation occurs, leading to a decrease in CO conversion [32]. This is reflected in the increase in activation energy for CO oxidation in the presence of $H_2$, from 13 to 34 kJ/mol. Similar results have been reported for

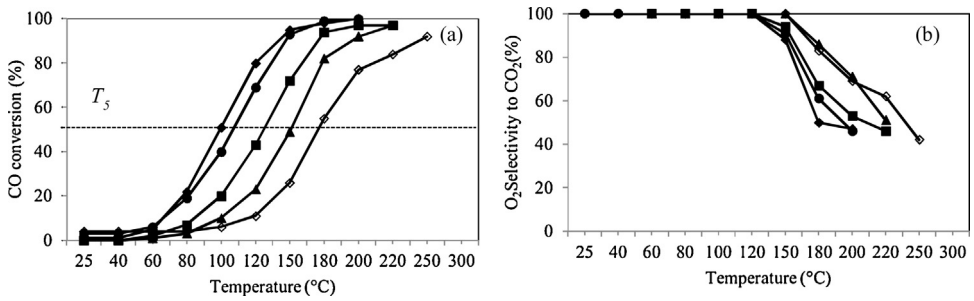


**Fig. 11.** (a) CO conversion and (b) selectivity as a function of temperature over ceria-based catalysts in PROX reaction. ◊ = $Ce_{0.9}Co_{0.10}O_{2-\delta}$, ▲ = $Ce_{0.89}$ $Cu_{0.01}Co_{0.10}O_{2-\delta}$, ■ = $Ce_{0.87}Cu_{0.03}Co_{0.10}O_{2-\delta}$, ● = $Ce_{0.85}Cu_{0.05}Co_{0.10}O_{2-\delta}$ and ♦ = $Ce_{0.95}Cu_{0.05}O_{2-\delta}$. Experimental conditions: λ = 2, GHSV = 48000 $h^{-1}$.

**Table 2**
Comparison of specific rates and activation energies under TOX and PROX.

| Catalyst | Specific rate at 150 °C (mol.$g^{-1}$ $s^{-1}$) x$10^{-4}$ | | Activation energy(kJ/mol) | |
|---|---|---|---|---|
| | TOX | PROX | TOX | PROX |
| $Ce_{0.90}Co_{0.10}O_{2-\delta}$ | 1.81 | 0.90 | 13 | 34 |
| $Ce_{0.89}Co_{0.10}$ $Cu_{0.01}O_{2-\delta}$ | 1.04 | 1.70 | 59 | 58 |
| $Ce_{0.87}Co_{0.10}$ $Cu_{0.03}O_{2-\delta}$ | 1.67 | 2.50 | 56 | 60 |
| $Ce_{0.85}Co_{0.10}$ $Cu_{0.05}O_{2-\delta}$ | 3.26 | 3.23 | 43 | 42 |
| $Ce_{0.95}Cu_{0.05}O_{2-\delta}$ | 3.30 | 3.30 | 72 | 71 |

CO oxidation over bulk $Co_3O_4$ [68]. The fact that the CO oxidation over Cu-containing catalysts is not adversely affected by the presence of $H_2$ supports the proposition that $H_2$ and CO oxidation reactions occur on independent sites on such catalysts [69]. Consequently, the calculated activation energies of these catalysts are almost the same for both TOX and PROX (Table 2). In the case of $Ce_{0.89}Cu_{0.01}Co_{0.10}O_{2-\delta}$ and $Ce_{0.87}Cu_{0.03}Co_{0.10}O_{2-\delta}$, the improved CO conversion under reducing conditions may be due to the existence of reduced Ce and Cu species ($Ce^{3+}$, $Cu^{+}$) which have been reported to facilitate CO oxidation [70]. The presence of $Ce^{3+}$ species is evident from the Ce(3d) XPS of the pre-reduced sample. The reaction profiles show that most of the $O_2$ consumption over Cu-containing catalysts is associated with the CO oxidation reaction and a minimal portion is consumed through the $H_2$ oxidation reaction, as revealed by high $O_2$ to $CO_2$ selectivity. However, $H_2O$ formation becomes more pronounced at temperatures exceeding 180 °C, leading to higher $O_2$ conversion. The superior catalytic behaviour of Cu-containing samples in PROX correlate well with the $H_2$-TPR profiles. The reducibility of the catalysts is improved as the Cu loading is increased, suggesting a possible strong interaction between Cu and Ce which in turn promotes oxygen mobility in the catalysts.

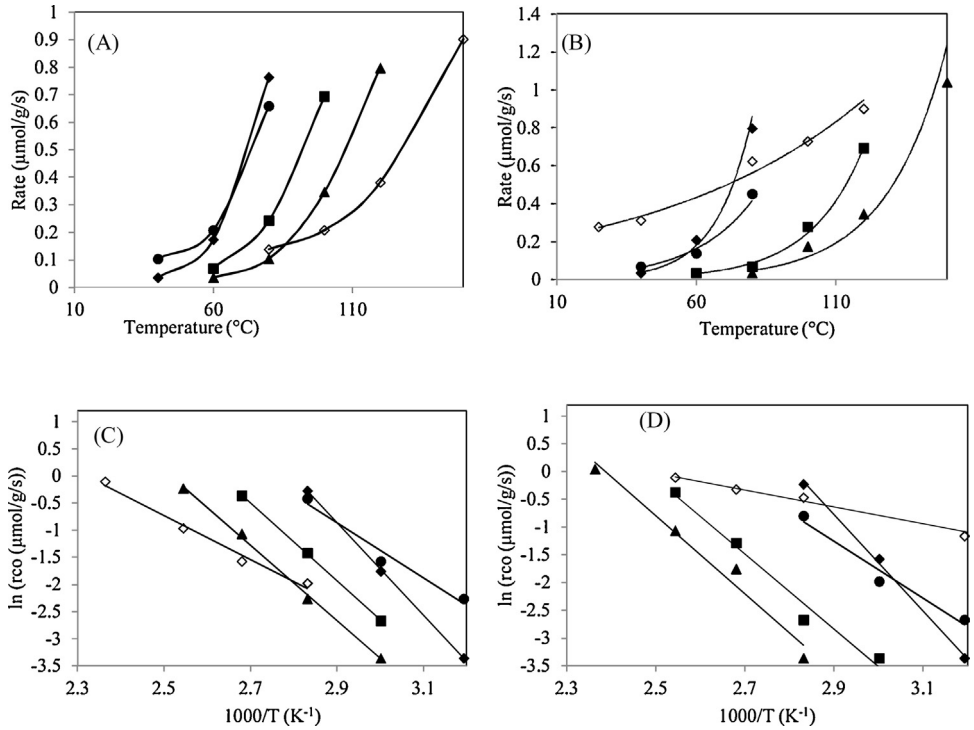


**Fig. 12.** Rate of the reaction as a function of temperature for (A) CO-PROX, (B) TOX and Arrhenius plots for (C) CO-PROX, (D) TOX studies. ◊ = $Ce_{0.9}Co_{0.10}O_{2-\delta}$, ▲ = $Ce_{0.89}$ $Cu_{0.01}Co_{0.10}O_{2-\delta}$, ■ = $Ce_{0.87}Cu_{0.03}Co_{0.10}O_{2-\delta}$, ● = $Ce_{0.85}Cu_{0.05}Co_{0.10}O_{2-\delta}$ and ♦ = $Ce_{0.95}Cu_{0.05}O_{2-\delta}$.

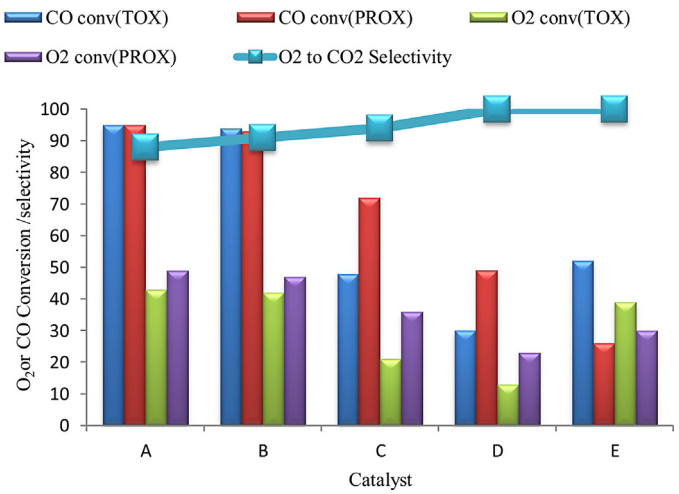


**Fig. 13.** Comparison of catalytic activities of A: $Ce_{0.95}Cu_{0.05}O_{2-\delta}$, B: $Ce_{0.85}Cu_{0.05}Co_{0.10}O_{2-\delta}$, C: $Ce_{0.87}Cu_{0.03}Co_{0.10}O_{2-\delta}$, D: $Ce_{0.89}Cu_{0.01}Co_{0.10}O_{2-\delta}$ and E: $Ce_{0.9}Co_{0.10}O_{2-\delta}$. Conditions: temperature = 150 °C, 48000 $h^{-1}$, λ = 2.

### 3.4.3. *Stability of the prepared catalysts and the effect of $H_2$ and $CO_2$*

The stability of the Co-based catalysts in a reducing environment has been cited as a concern due to reduction of Co to a lower valence state which is not active for CO oxidation [20]. Taking this into account, the stability of the catalysts was evaluated in the absence and presence of $CO_2$ and/or $H_2O$. Fig. 14 shows that all catalysts are quite stable under PROX conditions, showing no significant loss in activity and unchanged selectivity (≥50%) within the studied time-on-stream (24 h). This suggests that the active components of the catalysts do not get transformed to inactive species under present experimental conditions. Interestingly, at the reaction temperature of 180 °C, where time-on-stream experiments were conducted, $CO_2$ selectivity values of $Ce_{0.95}Cu_{0.05}O_{2-\delta}$ (50%), $Ce_{0.85}Cu_{0.05}Co_{0.10}O_{2-\delta}$ (63%) and $Ce_{0.87}Cu_{0.03}Co_{0.10}O_{2-\delta}$ (72%) are not comparable, although their CO conversion values are within ±5%. The exact CO conversions observed over these respective catalysts are 96, 95 and 92%, possibly due to the presence of different metal ion species' over Cu and Co–Cu catalysts.

Although the PROX studies conducted with only CO, $H_2$ and $O_2$ provide valuable understanding of the catalyst performance, it is necessary to evaluate catalytic behaviour in the presence of $H_2O$ and $CO_2$, since these components are found in $H_2$-rich gas obtained from steam reforming. Hence, the stability of the catalysts was also investigated in the presence of 7 vol% $H_2O$ and 15 vol% $CO_2$ (Fig. 14), using the aforementioned conditions, with varied $N_2$ levels to compensate for the introduction of $H_2O$ and $CO_2$. These conditions fit within the parameters that are commonly employed for laboratory scale PROX experiments [5,14].

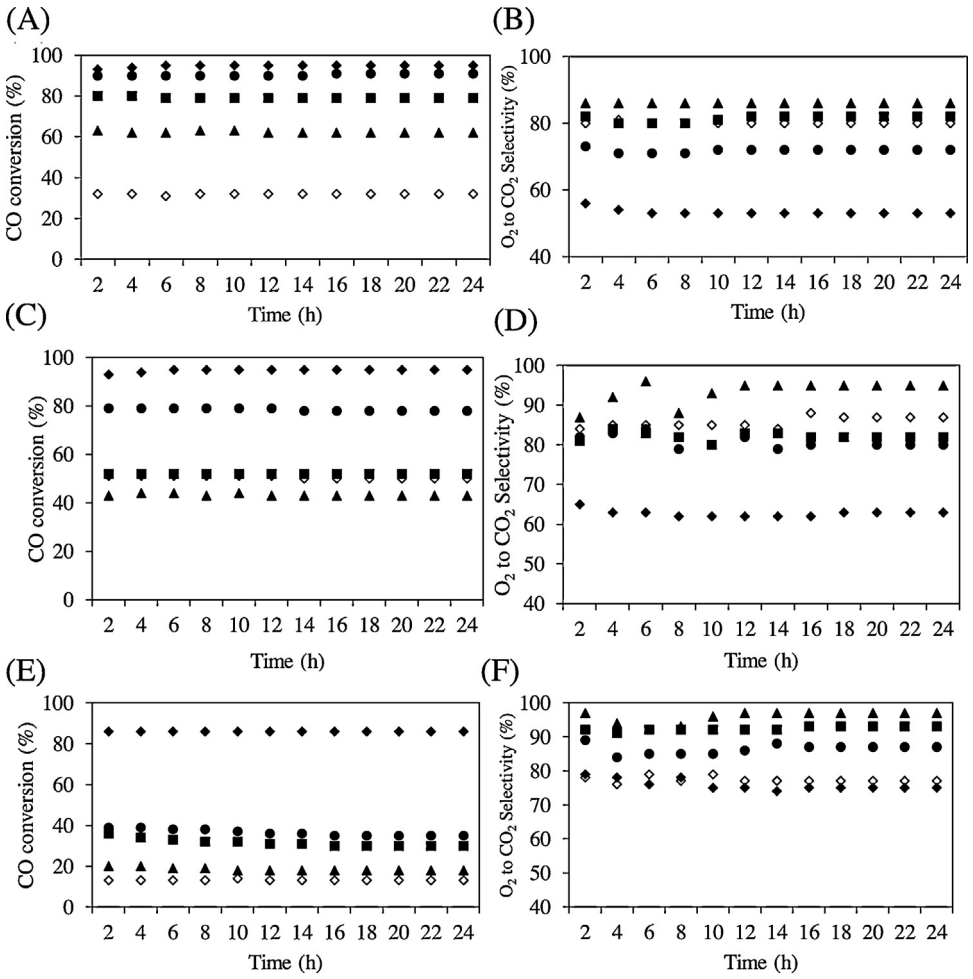


**Fig. 14.** Time-on-stream CO conversion and selectivity on ceria-based catalysts at 180 °C in the presence of 15 vol% $CO_2$ (A, B) (dry PROX), in the presence of 7 vol% $H_2O$ (C, D) and in 7 vol% $H_2O$ + 15 vol% $CO_2$ (E,F). ◊ = $Ce_{0.9}Co_{0.10}O_{2-\delta}$, ▲ = $Ce_{0.89}Cu_{0.01}Co_{0.10}O_{2-\delta}$, ■ = $Ce_{0.87}Cu_{0.03}Co_{0.10}O_{2-\delta}$, ● = $Ce_{0.85}Cu_{0.05}Co_{0.10}O_{2-\delta}$ and ♦ = $Ce_{0.95}Cu_{0.05}O_{2-\delta}$. At λ = 2, GHSV = 12 000 $h^{-1}$ for $Ce_{0.9}Co_{0.10}O_{2-\delta}$ and 48 000 $h^{-1}$ for all other catalysts.

As shown in Fig. 14(A–F), the introduction of $H_2O$ and/or $CO_2$ has a negative effect on the catalytic activity of the Co-based and bimetallic catalysts. The extent of deactivation in the presence of $CO_2$ appears to be higher for the $Ce_{0.9}Co_{0.10}O_{2-\delta}$ catalyst compared to its bimetallic analogues. In the presence of 15 vol% $CO_2$, CO conversion over $Ce_{0.90}Co_{0.10}O_{2-\delta}$ decreases from 90% to 32% (Fig. S6), although the selectivity is slightly improved from 72% to 80%. Under the same reaction conditions, CO conversion drops from 81 to 62%, 92 to 79% and 95 to 90% over $Ce_{0.89}Cu_{0.01}Co_{0.10}O_{2-\delta}$, $Ce_{0.87}Cu_{0.03}Co_{0.10}O_{2-\delta}$ and $Ce_{0.85}Cu_{0.05}Co_{0.10}O_{2-\delta}$, respectively. Notably, the negative effect associated with the presence of $CO_2$ is moderate for Co-Cu catalysts and becomes less as Cu content is increased. However, the deactivation related to the introduction of 7 vol% $H_2O$ (in the absence of $CO_2$) is more pronounced relative to that induced by $CO_2$ on the Co-Cu catalysts. In contrast, water is less detrimental, compared to $CO_2$, on the activity of $Ce_{0.90}Co_{0.10}O_{2-\delta}$. The PROX activity and corresponding selectivity of the investigated catalysts under the different gas compositions are summarized in Table 3.

The addition of both $CO_2$ and $H_2O$ result in lower catalytic performance of these catalysts. From Fig. 14, it is clear that the degree of deactivation is reduced as the amount of Cu present in the catalyst is increased. Under these reaction conditions, $Ce_{0.90}Co_{0.10}O_{2-\delta}$ only reached CO conversion of 13%. As Cu content of 1, 3 and 5 at% is incorporated, the CO conversion is improved to 18, 31 and 36%. This suggests that the Cu active sites do not greatly change in the presence of either $H_2O$ and/or $CO_2$. Accordingly, the activity of $Ce_{0.95}Cu_{0.05}O_{2-\delta}$ is not significantly affected by the presence of $H_2O$ and/or $CO_2$. In the presence of both 7 vol% $H_2O$ and 15 vol% $CO_2$, this catalyst achieved 86% CO conversion and 75% selectivity. It is noteworthy that all the catalysts can fully regain their performance by switching to a $H_2O/CO_2$-free feed, which shows that the deactivation is reversible. In the presence of $CO_2$ and/or $H_2O$, the selectivity of $O_2$ to $CO_2$ is improved for all studied materials, monometallic and bimetallic catalysts. This observation is accompanied by a decrease in $H_2$ consumption. Such results confirm that a decrease in CO conversion under these conditions is not caused by the reverse water gas shit reaction (RWG: $CO_2 + H_2 \rightarrow CO + H_2O$). Consistently, the reactions performed using a feed of 15 vol% $CO_2$ and 50 vol% $H_2$ showed neither $H_2$ nor $CO_2$ conversion, ruling out the occurrence of reverse water gas shift or methanation reactions. The deactivation behaviour brought about the presence of $H_2O$ can be ascribed to the adsorption of water on the catalyst surface, leading to a blockage of the active sites. The formation of a CO–$H_2O$ complex has also been suggested as the possible explanation for reduced activity of such catalysts under similar conditions [71,72]. The negative effect of introducing $CO_2$ into the feed can be attributed to the competitive adsorption, between CO and $CO_2$, at the active sites. Since the only active sites for CO oxidation appear to be $Co^{2+}$ ions in $Ce_{0.90}Co_{0.10}O_{2-\delta}$, the effect of $CO_2$ and/or $H_2O$ is more pronounced due to the disturbance of the redox circle [71,72].

## 4. Conclusions

In this work, $Ce_{0.90}Co_{0.10}O_{2-\delta}$ and $Ce_{0.90-x}Cu_xCo_{0.10}O_{2-\delta}$ ($x = 0.01$, 0.03 and 0.05) catalysts were synthesized using a urea-assisted combustion method and evaluated for total and preferential CO oxidation. The resulting catalysts are single-phase nanocrystalline materials with a fluorite structure. Catalytic activity of $Ce_{0.90}Co_{0.10}O_{2-\delta}$ could be significantly enhanced by the addition of Cu, for TOX and PROX. The improvement in the activity has a direct relationship with the increased reducibility, which could be linked to better oxygen mobility due to Ce–Cu interactions. All catalysts are stable, highly selective and able to achieve complete CO conversion under different reaction conditions. Importantly, Cu-containing catalysts do not experience a drop in CO conversion in the presence of $H_2$, signalling that $H_2$ and CO conversion may be taking place at independent sites. For bimetallic Co–Cu catalysts, it is assumed that CO oxidation predominantly takes place on the Cu site, while $H_2$ oxidation mainly occurs on the Co site. Co-containing catalysts were found to have a low tolerance for $CO_2$ and $H_2O$ due to competitive adsorption and blockage of the active sites. However, the $CO_2/H_2O$ tolerance improves with increasing Cu loading.

## Acknowledgements

The authors gratefully acknowledge the Department of Science and Technology (DST), South Africa, and Mintek (Advanced Metals Initiative program) for financial support. The authors are also thankful to Professor M.S. Hegde, SSCU and the Indian Institute of Science (Bangalore) for their help with XPS recording and discussion.

## Appendix A. Supplementary data

Supplementary data associated with this article can be found, in the online version, at http://dx.doi.org/10.1016/j.apcatb.2015.08.043.

## References

[1] Y. Wang, K.S. Chen, J. Mishler, S.C. Cho, X.C. Adroher, Appl. Energy 88 (2011) 981–1007.
[2] G. Hoogers, Fuel Cell Technology Handbook, CRC Press LLC, Boca Raton, Florida, 2003.
[3] G. Hoogers, Fuel Cell Technology Handbook, in: G. Hoogers (Ed.), CRC Press LLC, Boca Raton, Florida, 2003, pp. 5/1-5/23.
[4] D. Thompsett, Fuel Cell Technology Handbook, CRC Press LLC, Boca Raton, in: G. Hoogers (Ed.), Florida (2003), pp. 6 /1-6/ 22.
[5] A. Mishra, R. Prasad, Bull. Chem. React. Eng. Catal. 6 (2011) 1–14.
[6] G. Avgouropoulos, T. Ioannides, Appl. Catal. A 244 (2003) 155–167.
[7] T.A. Zepeda, A. Martinez-Hernandez, R. Guil-Lopez, B. Pawelec, Appl. Catal. B 100 (2010) 450–462.
[8] J.G.E. Cohn, Carbon Monoxide Removal from Hydrogen-containing Gases, Engelhard Industries, Inc., 1965, p. 3.
[9] K. Liu, A. Wang, T. Zhang, ACS Catal. 2 (2012) 1165–1178.
[10] D. Duprez, C. Descorme, Catalysis by Ceria and Related Materials, in: A. Trovarelli (Ed.), 2nd ed., Imperial College Press; Distributed by World Scientific, London, 2013, pp. 243–280.
[11] M. Shelef, G.W. Graham, R.W. McCabe, Catalysis by Ceria and Related Materials, in: A. Trovarelli (Ed.), Imperial College Press; Distributed by World Scientific, London, 2013, pp. 343–375.
[12] M.S. Hegde, G. Madras, K.C. Patil, Acc. Chem. Res. 42 (2009) 704–712.
[13] A. Martinez-Arias, A.B. Hungría, G. Munuera, D. Gamarra, Appl. Catal. B 65 (2006) 207–216.
[14] A. Gomez-Cortes, Y. Marquez, J. Arenas-Alatorre, G. Diaz, Catal. Today 133–135 (2008) 743–749.
[15] T. Tabakova, M. Manzoli, F. Vindigni, V. Idakiev, F. Boccuzzi, J. Phys. Chem. A 114 (2009) 3909–3915.
[16] S.K. Meher, M. Cargnello, H. Troiani, T. Montini, G.R. Rao, P. Fornasiero, Appl. Catal. B 130–131 (2013) 121–131.
[17] R.V. Gulyaev, A.I. Stadnichenko, E.M. Slavinskaya, A.S. Ivanova, S.V. Koscheev, A.I. Boronin, Appl. Catal. A 439–440 (2012) 41–50.
[18] W. Liu, M. Flytzanistephanopoulos, J. Catal. 153 (1995) 304–316.
[19] W. Liu, M. Flytzanistephanopoulos, J. Catal. 153 (1995) 317–332.
[20] Y. Teng, H. Sakurai, A. Ueda, T. Kobayashi, Int. J. Hydrogen Energy 24 (1999) 355–358.
[21] W. Liu, M. Flytzani-Stephanopoulos, Chem. Eng. J. 64 (1996) 283–294.
[22] A.A. Firsova, A.N. Ilichev, T.I. Khomenko, L.V. Gorobinskii, Y.V. Maksimov, I.P. Suzdalev, V.N. Korchak, Kinet. Catal. 48 (2007) 282–291.
[23] A.A. Firsova, T.I. Khomenko, A.N. Ilichev, V.N. Korchak, Kinet. Catal. 49 (2008) 682–691.
[24] G. Sedmak, S. Hočevar, J. Levec, J. Catal. 222 (2004) 87–99.
[25] G.G. Jernigan, G.A. Somorjai, J. Catal. 147 (1994) 567–577.
[26] H.K. Lin, H.C. Chiu, H.C. Tsai, S.H. Chien, C.B. Wang, Catal. Lett. 88 (2003) 169–174.
[27] Y.F.Y. Yao, J. Catal. 33 (1974) 108–122.
[28] K. Omata, Y. Kobayashi, M. Yamada, Catal. Commun. 6 (2005) 563–567.
[29] W.H. Yang, M.H. Kim, S.-W. Ham, Catal. Today 123 (2007) 94–103.
[30] T. Bao, Z. Zhao, Y. Dai, X. Lin, R. Jin, G. Wang, T. Muhammad, Appl. Catal. B 119–120 (2012) 62–73.

[31] P. Gawade, B. Bayram, A.-M.C. Alexander, U.S. Ozkan, Appl. Catal. B 128 (2012) 21–30.
[32] M.P. Woods, P. Gawade, B. Tan, U.S. Ozkan, Appl. Catal. B 97 (2010) 28–35.
[33] L.F. Liotta, G. Di Carlo, G. Pantaleo, A.M. Venezia, G. Deganello, Appl. Catal. B 66 (2006) 217–227.
[34] J. Jansson, A.E.C. Palmqvist, E. Fridell, M. Skoglundh, L. Osterlund, P. Thormählen, V. Langer, J. Catal. 211 (2002) 387–397.
[35] Z. Zhao, R. Jin, T. Bao, H. Yang, X. Lin, G. Wang, Int. J. Hydrogen Energy 37 (2012) 4774–4786.
[36] L.F. Liotta, G. Di Carlo, G. Pantaleo, G. Deganello, Appl. Catal. B 70 (2007) 314–322.
[37] M. Narayanappa, V.D.B.C. Dasireddy, H.B. Friedrich, Appl. Catal. A 447–448 (2012) 135–143.
[38] P. Bera, A. Gayen, M.S. Hegde, N.P. Lalla, L. Spadaro, F. Frusteri, F. Arena, J. Phys. Chem. B 107 (2003) 6122–6130.
[39] T. Baidya, A. Gayen, M.S. Hegde, N. Ravishankar, L. Dupont, J. Phys. Chem. B 110 (2006) 5262–5272.
[40] C. Liu, Q. Liu, L. Bai, A. Dong, G. Liu, S. Wen, J. Mol. Catal. A 370 (2013) 1–6.
[41] J. Jiang, L. Li, Mater. Lett. 61 (2007) 4894–4896.
[42] S. Tsunekawa, K. Ishikawa, Z.-Q. Li, Y. Kawazoe, A. Kasuya, Phys. Rev. Lett. 85 (2000) 3440–3443.
[43] X.D. Zhou, W. Huebner, Appl. Phys. Lett 79 (2001) 3512–3514.
[44] F. Zhang, S.W. Chan, J.E. Spanier, E. Apak, Q. Jin, R.D. Robinson, I.P. Herman, Appl. Phys. Lett 80 (2002) 127–129.
[45] M. Fernandez-Garcia, A. Martinez-Arias, J.C. Hanson, J.A. Rodriguez, Chem. Rev. 104 (2004) 4063–4104.
[46] A. Gupta, U.V. Waghmare, M.S. Hegde, Chem. Mater. 22 (2010) 5184–5198.
[47] P. Sudarsanam, B. Mallesham, P.S. Reddy, D. Großmann, W. Grünert, B.M. Reddy, Appl. Catal. B 144 (2014) 900–908.
[48] L. Li, G. Li, Y. Che, W. Su, Chem. Mater. 12 (2000) 2567–2574.
[49] J.E. Spanier, R.D. Robinson, F. Zhang, S.-W. Chan, I.P. Herman, Phys. Rev. B 64 (2001) 245407.
[50] B. Holland, J. Porous Mater. 10 (2003) 17–22.
[51] M.F. Luo, Y.J. Zhong, X.X. Yuan, X.M. Zheng, Appl. Catal. A 162 (1997) 121–131.
[52] D. Gamarra, A. Hornes, Z.s Koppany, G. Schay, J. Munuera, A. Martinez-Arias, J. Power Sources 169 (2007) 110–116.
[53] T. Caputo, L. Lisi, R. Pirone, G. Russo, Appl. Catal. A 348 (2008) 42–53.
[54] D. Gamarra, A. Lopez Camara, M. Monte, S.B. Rasmussen, L.E. Chinchilla, A.B. Hungria, G. Munuera, N. Gyorffy, Z. Schay, V. Cortes Corberán, J.C. Conesa, A. Martinez-Arias, D. Appl, Catal. B 130–131 (2013) 224–238.
[55] T. Baidya, M.S. Hegde, J. Gopalakrishnan, J. Phys. Chem. B 111 (2007) 5149–5154.
[56] Y. Nagai, T. Yamamoto, T. Tanaka, S. Yoshida, T. Nonaka, T. Okamoto, A. Suda, M. Sugiura, Catal. Today 74 (2002) 225–234.
[57] S. Sun, X. Zhao, H. Lu, Z. Zhang, J. Wei, Y. Yang, Cryst. Eng. Commun. 15 (2013) 1370–1376.
[58] B.B. Tope, R.J. Balasamy, A. Khurshid, L.A. Atanda, H. Yahiro, T. Shishido, K. Takehira, S.S. Al-Khattaf, Appl. Catal. A 407 (2011) 118–126.
[59] P. Burroughs, A. Hamnett, A.F. Orchard, G. Thornton, J. Chem. Soc. Dalton Trans. (1976) 1686–1698.
[60] M. Kang, M. Song, K. Kim, React. Kinet. Catal. Lett. 79 (2003) 3–10.
[61] A. Gayen, T. Baidya, G.S. Ramesh, R. Srihari, M.S. Hegde, J. Chem. Sci. 118 (2006) 47–55.
[62] J. Beckers, G. Rothenberg, Green Chem. 12 (2010) 939–948.
[63] S. Royer, D. Duprez, ChemCatChem 3 (2011) 24–65.
[64] Z. Zhao, X. Lin, R. Jin, G. Wang, T. Muhammad, Appl. Catal. B 115–116 (2012) 53–62.
[65] S. Scire, C. Crisafulli, P.M. Riccobene, G. Patane, A. Pistone, Appl. Catal. A 417–418 (2012) 66–75.
[66] R. Prasad, G. Rattan, Bull. Chem. React. Eng. Catal. 5 (2010) 7–30.
[67] T. Bao, Z. Zhao, Y. Dai, X. Lin, R. Jin, G. Wang, T. Muhammad, Appl. Catal. B 119–120 (2012) 62–73.
[68] Y.J. Chen, D.E. Wu, C.T. Yeh, Rev. Adv. Mater. Sci. 5 (2003) 41–46.
[69] H.C. Lee, D.H. Kim, Catal. Today 132 (2008) 109–116.
[70] A. Martinez-Arias, D. Gamarra, M. Fernandez-Garcia, A. Hornes, C. Belver, Top. Catal. 52 (2009) 1425–1432.
[71] Q. Guo, S. Chen, Y. Liu, Y. Wang, Chem. Eng. J. 165 (2010) 846–850.
[72] D. Gamarra, A. Martinez-Arias, J. Catal. 263 (2009) 189–195.